1st examiner Dr. Daniel S. Margulies
Neuroanatomy and Connectivity
Max Planck Institute for Human Cognitive
and Brain Sciences, Leipzig

2nd examiner Prof. Dr. Felix Blankenburg
Neurocomputation and Neuroimaging
Department for Psychology
Free University of Berlin

Evaluating nonlinear coregistration of BOLD EPI and T1w images

Master Thesis

In partial fulfillment of the Master of Science

Social, Cognitive, Affective Neuroscience

Julia Huntenburg, ID 4686947
Leuthener Str. 5, 10829 Berlin
ju.huntenburg@gmail.com

Abstract

In view of geometric distortions in EPI images, correction methods are required to enable accurate mapping to the brain anatomy. Nonlinear coregistration constitutes an interesting alternative in the absence of gold-standard correction approaches such as fieldmapping and reverse phase encoding. Although early investigations of nonlinear coregistration have yielded encouraging results, the method has not been widely adopted for neuroimaging analysis due to the lack of extensive evaluation and user-friendly implementation. Here, the usefulness of direct, nonlinear BOLD EPI and T1w image coregistration for standard applications is explored. A practicable framework is provided through the integration of required preprocessing steps and nonlinear transformation with Advanced Normalization Tools (ANTs) in a single Nipype workflow. Different versions of the pipeline were tested on a large set of real imaging data as well as on simulated data. In a direct comparison to existing methods no satisfactory results could be obtained for nonlinear coregistration. In particular, a lack of robustness across datasets challenges the viability of nonlinear coregistration for distortion correction on a larger scale and highlights the importance of extensive evaluation procedures.

Keywords: nonlinear coregistration, distortion correction

Introduction

In functional magnetic resonance imaging (fMRI), coregistration of functional time series to a high resolution anatomical image is crucial for accurate localization (Toga & Thompson 2001; Brett et al. 2002). Classical implementations of intrasubject, intermodal registration rely on linear transformation algorithms, assuming that geometric proportions remain constant across imaging modalities. Unlike structural images, functional scans often suffer from distortions, rendering the supposition of geometric consistency partially invalid (Jezzard & Clare 1999). To overcome the effect of distortion bias in functional images, linear transformations need to be supplemented with appropriate methods for distortion correction (Hutton et al. 2002; Jezzard 2012). While existing correction techniques based on fieldmaps (Jezzard & Balaban 1995; Weisskoff & Davis 1992) and reverse phase encoding (Andersson et al. 2003) achieve good results, they naturally entail certain limitations. Nonlinear transformation algorithms have been suggested as an alternative approach for distortion correction (Kybic et al. 2000; Studholme et al. 2000; Gholipour et al. 2008a). Yet, large-scale evaluation and application-friendly implementation of this method remain outstanding issues.

Geometric distortions in EPI images

The majority of current fMRI studies rely on blood oxygen level dependent (BOLD) (Ogawa et al. 1990) echo planar imaging (EPI) sequences (Mansfield 1977). These provide the temporal resolution required to track functional dynamics at the cost of high susceptibility to magnetic field inhomogeneities. Inevitably, the presence of a subject in the scanner introduces inhomogeneities in the static magnetic field (B0) as well as the superimposed gradient fields, which cannot be completely overcome by shimming (Cusack et al. 2003). It is thus a well recognized problem that EPI images suffer from geometric distortions due to nonlinearity of spatial encoding gradients (Jezzard 2012). Driven by high susceptibility differences, distortions particularly affect brain regions near bones or air filled sinuses such as orbitofrontal cortex (OFC) and the temporal lobes. Because phase errors accumulate over time, distortions are substantially scaled up in the direction of phase encoding where the time between acquisition of adjacent voxels is greatest. Here, shifts can be augmented to the order of several voxels (Jezzard & Balaban 1995). The erroneous signal displacement severely

compromises coregistration to structural images and can eventually impair functional analysis in respective areas (Villain et al. 2010).

Fieldmaps and reverse phase encoding

A popular approach to counteract distortion artefacts employs explicit, individual maps of B0 inhomogeneities (Jezzard & Balaban 1995; Weisskoff & Davis 1992; Chen & Wyrwicz 1999; Reber et al. 1998). Those so called fieldmaps are derived based on the phase shift between two non-EPI scans with a slight echo time offset and then used to unwarp the distorted EPI image along the phase encoding direction. More recently it has been suggested that an EPI scan with a reverse phase encoding gradient and opposite distortions from the time series can be used to derive an off-resonance field for a similar correction (Andersson et al. 2003; Holland et al. 2010). However, some constraints of the aforementioned approaches persist. Both methods require additional scanning time and prospective planning, the latter precluding application to existing data. The fidelity of correction will vary with the quality of the additional scans as faithful reconstruction of fieldmaps from phase information depends on the noise level of the images (Hutton et al. 2002). Moreover, accuracy of the correction cannot necessarily be assumed in the presence of strong inhomogeneities as shown for fieldmaps by Wu and colleagues (Wu et al. 2008).

Nonlinear coregistration

Alternatively, the deformation required for distortion correction can be derived directly through nonlinear coregistration of EPI and T1w images[1] (Kybic et al. 2000; Studholme et al. 2000; Gholipour et al. 2008a). Nonlinear algorithms are widely used for intersubject, intramodal registration problems but their adaption for EPI and T1w coregistration poses serious challenges. Different image contrasts between modalities require additional preprocessing and restrict the choice of similarity metrics (Bhushan et al. 2012). Moreover, limited structural information in EPI images makes it extremely difficult to establish faithful correspondence to the anatomy. It is therefore crucial to prevent unreasonable displacement

[1] While the focus here are distortions in BOLD EPI images, similar issues pertain to the use of EPI sequences in diffusion weighted imaging (DWI). Interestingly, the idea of nonlinear coregistration has been explored more extensively in DWI (Wu et al. 2008; Tao et al. 2009; Bhushan et al. 2012; Daga et al. 2013). It remains unclear how the outcomes translate between imaging modalities.

by imposing constraints on the deformation field (Gholipour et al. 2007). Previous studies for instance informed their transformation model with physics-based constraints concerning the smoothness of the deformation field (Studholme et al. 2000) and restricted deformations largely to phase encoding direction (Gholipour et al. 2008a). While the results of those procedures are generally encouraging, they have not made it to common practice fMRI analysis. Potential reasons include the lack of large-scale evaluation and availability in common neuroimaging software. Moreover, additional scans are often required, involving similar problems as field based methods.

The present study addresses some of the issues potentially arresting the adoption of nonlinear coregistration beyond a specialized community. It explores the possibility of direct nonlinear coregistration between EPI and T1w images within a user-friendly pipeline, exclusively employing common neuroimaging software. Performance and robustness of the correction are evaluated based on a large real dataset as well as simulated data in comparison to established correction techniques.

Methods

Data acquisition

Neuroimaging data of 73 healthy participants (31.6 ± 16.3 years old, 36 female) from the Leipzig Cohort for Mind-Body-Emotion Interactions (LEMON) was included in the study. The subjects gave informed consent and all protocols were approved by the local ethics committee at the University of Leipzig, Faculty of Medicine. Data was acquired on a 3 Tesla Siemens Verio Scanner using a 32 channel head coil. For each subject, a T1w anatomical image was acquired using a magnetization prepared two rapid acquisition gradient echo sequence (MP2RAGE, TR = 5 s, TE = 2.92 ms, TI_1 = 700 ms, TI_2 = 2500 ms, flip $angle_1$ = 4° , flip $angle_2$ = 5°, voxel size = 1 × 1 × 1 mm, FOV = 256 mm, 176 slices). Further, a BOLD weighted resting state time series containing 657 contiguous volumes was collected with a gradient echo EPI sequence (TR = 1.4 s, TE = 30 ms, flip angle = 69°, multiband factor = 4, voxel size = 2.3 × 2.3 × 2.3 mm, FOV = 202 mm, 64 slices, phase encoding = anterior-posterior (AP)). A pair of gradient echo non-EPI scans (TR = 0.68 s, TE_1 = 5.19 ms, TE_2 = 7.65 ms, flip angle = 60°, voxel size = 2.3 × 2.3 × 2.3 mm, FOV = 202 mm, 64 slices) and two sets of spin echo EPI scans (TR = 2.2 s, TE = 50 ms, flip angle = 90°, multiband

factor = 4, voxel size = 2.3 × 2.3 × 2.3 mm, FOV = 202 mm, 64 slices, phase encoding = AP, 3 volumes / PA, 3 volumes) were acquired for fieldmap and reverse phase encoding correction, respectively.

Image processing

To ensure reproducibility and enable smooth interfacing of different neuroimaging software, all data processing was streamlined using Nipype[2] (Gorgolewski et al. 2011). An overview of the processing pipeline is shown in Figure 1a. Brain extraction of T1w images was performed with MIPAV[3] (McAuliffe et al. 2001) in JIST environment[4] (Lucas et al. 2010) employing CBS Tools MP2RAGE Background Masking (Bazin et al. 2014) and the SPECTRE 2010 algorithm (Carass et al. 2011). Subsequently, cortical reconstruction and volumetric segmentation was performed with Freesurfer (Dale et al. 1999; Fischl et al. 1999). Transformation into standard space (MNI152, voxel size = 1 × 1 × 1 mm) was derived using ANTs[5] (Avants et al. 2011). Functional images were realigned to the first volume using FSL MCFLIRT (Jenkinson et al. 2002). A temporal average of the motion corrected time series was used for rigid coregistration to the subject's T1w image, carried out with a combination of FSL FLIRT (Jenkinson & Smith 2001) and Freesurfer bbregister (Greve & Fischl 2009). Distortion correction was either omitted *(uncorrected)* or carried out employing one out of

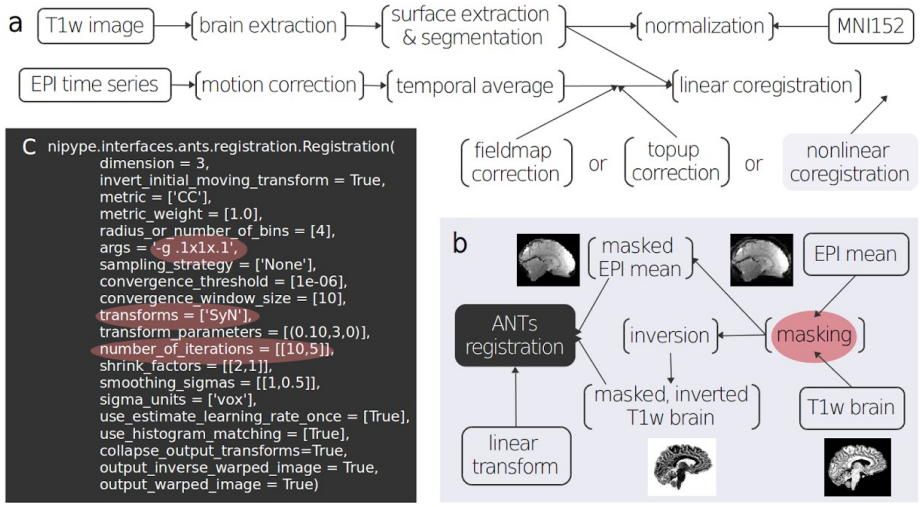

Figure 1. Image processing pipeline. Basic processing steps are schematically shown in **a**; **b** depicts the pipeline for nonlinear coregistration in more detail. Inputs are marked by closed outlines. Input parameters to the core node for nonlinear registration with ANTs are listed in **c** (here for v3, see Tab.2). Parameters that are varied between different versions of nonlinear correction are highlighted in pink.

[2] http://nipy.sourceforge.net/nipype/
[3] http://mipav.cit.nih.gov/index.php
[4] http://www.nitrc.org/projects/jist/
[5] http://stnava.github.io/ANTs/

three different methods described below (*fieldmap, topup, nonlinear)*. Finally, transformations from distortion correction and coregistration were collapsed and applied to the temporal mean image in a single interpolation. Where necessary, the mean image was further projected into standard space using the transformation derived from the anatomical data before.

B0 field based distortion correction (fieldmap). Correction based on explicit mapping of B0 field inhomogeneities was carried out using the fsl_prepare_fieldmap script and FUGUE (Jenkinson et al. 2012). The phase image was scaled to radians per second, phase unwrapped and tightly masked. The resulting fieldmap was converted into a map of shift values in voxel space (shiftmap) and unmasked to avoid edge effects. The mean functional image was registered to the magnitude image and unwarped using the shiftmap before coregistration to the anatomy.

Reserve phase encoding based distortion correction (topup). FSL TOPUP (Smith et al. 2004) was used to derive the off-resonance field from sets of images with reverse phase encoding direction (Andersson et al. 2003). Processing and application of this field followed the same steps as described for the B0 fieldmap above.

Nonlinear coregistration to anatomy for distortion correction (nonlinear). Nonlinear coregistration of the mean functional and T1w images was carried out with ANTs applying the symmetric diffeomorphic transformation model SyN and the fast cross-correlation similarity metric (Avants et al. 2008). Extensive testing was performed to find optimal preprocessing steps and ANTs parameter sets. After an initial exploratory phase a basic procedure was fixed, which is depicted in Figures 1b and c and available online as a reusable Nipype workflow and command line tool[6]. In short, the intensities of the brain extracted T1w image were scaled and inverted to resemble the contrast of of the functional image. Careful masking of EPI and T1w image preceded nonlinear coregistration, which was initiated with the rigid transformation derived before. Starting from this essential pipeline, systematic variation of four core aspects, namely masking, regularization, iterations and deformation restriction, ensued (see Tab. 1 for details). The second testing phase was accompanied by more formal evaluation as outlined in the *Evaluation* section below.

[6] https://github.com/NeuroanatomyAndConnectivity/epi_t1_nonlinear

Regularization	*SyN* : classical SyN implementation relying on Gaussian field regularization. *B-spline SyN* : SyN transformation model with regularization through fast B-spline approximation (spline order=3, base level grid=26 mm) (Tustison & Avants 2013).
Iterations	*Few* : two stage transformation, [10, 5] iterations, [1, 0.5] voxel smoothing, [2,1] shrinkage. *Many* : four stages, [100,70,50,20] iterations, [3,2,1] voxel smoothing, [6,4,2,1] shrinkage.
Masking	*Whole brain* : binarized and dilated Freesurfer aparc+aseg output image. *Fieldmap* : including only regions with large deformation values in independent fieldmap template (Gholipour et al. 2008b) (Supplementary Fig. 1).
Restriction	*Strict* : deformations exclusively restricted to y (phase encoding) direction. *Moderate* : restriction applying weight vector [0.1, 1, 0.1] for deformation in x,y,z direction.

Table 1 Variation of parameters in the nonlinear registration pipeline.

Simulation

An undistorted EPI image was simulated using FSL POSSUM (Drobnjak et al. 2010). Tissue class images were derived from one arbitrarily selected subject of the LEMON cohort (cf. *Data acquisition*) using FSL FAST (Zhang et al. 2001) to serve as the segmented anatomical voxel model. Pulse sequence information was set to standard values (TR = 3 s, TE = 30 ms, flip angle = 90°, voxel size = 4 × 4 × 3.6 mm, slice gap = 0.4 mm, FOV = 256 mm, 40 slices) and thermal noise was added for a resultant signal-to-noise ratio of 10. The image was blurred with a 2 mm Gaussian kernel. The subject's real fieldmap was used to introduce different levels of distortion using FSL FUGUE with echo spacing incrementing from 0.1 to 1 ms (Chambers et al. 2014; Bhushan et al. 2012) (Supplementary Fig. 3). Based on real data values, the images were clipped at an intensity of twice their robust maximum. Similar to the real data, the ten distorted images were registered to the subject's T1w image and either no *(uncorrected)*, *fieldmap* or *nonlinear* distortion correction was applied.

Evaluation

Measures and images for evaluation were derived and plotted in an automated fashion using Nipype, nibabel[7] and nilearn[8].

[7] http://nipy.org/nibabel/
[8] http://nilearn.github.io/

Visual inspection. Group averages of mean EPI images were created. To evaluate the fit to anatomical structures, edge images were derived from the subject's T1w image or the MNI152 template, respectively, consisting of grey-white matter boundaries and the brain mask outline. Intensity difference maps between the subjects' mean functional images after different forms of distortion correction were derived and combined into a group average map for each contrast. EPI masks were created from each subject's mean functional image using FSL BET (Smith 2002) and used to derive minimal and average group masks and group mask standard deviation. Deformation fields from the different correction methods were converted to a common format and scaled for comparability. As fieldmap and topup shiftmaps are restricted to one (the phase encoding) dimension, only this dimension could be considered for evaluation

Quantitative measures. Similarity of EPI and T1w images was assessed in terms of normalized mutual information (NMI) and correlation ratio (CR) within either a whole brain mask or orbitofrontal regions as defined by the Harvard-Oxford probabilistic atlas (>25%) (Supplementary Fig. 2). Voxelwise Spearman's rank correlation was calculated between the deformation fields and between the corrected mean functional images resulting from the different correction methods. Likewise, for the simulated data, correlation between the original distortion field and the nonlinear deformation field as well as correlation between the undistorted image and the differentially corrected images was computed for each level of distortion. The span between the robust minimum and maximum shift values was computed for the deformation fields across subjects or levels of distortion respectively.

Results

Contrary to initial expectations, single parameter variations exhibited a complex patterning of negative and positive consequences throughout optimization of nonlinear coregistration. While an exhaustive account of the tested procedures is beyond the scope of this paper, the following section describes a comparative evaluation of a subselection of nonlinear coregistration pipelines along with the established correction methods. The selection was made to provide a comprehensive picture of the impact of core parameters (see Tab. 1). The results of all possible combinations of parameters can be found in the Supplementary Material.

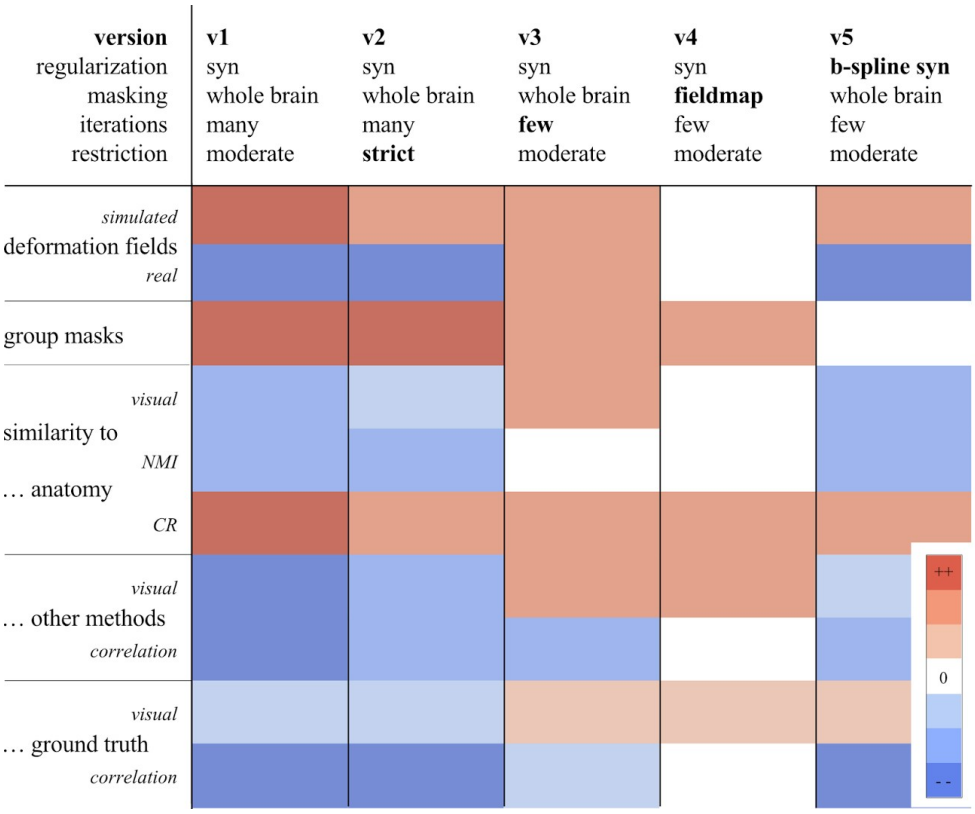

Table 2 Versions of nonlinear registration. The five parameters settings discussed in the main text are arranged in columns; rows represent the different outcome measures. The cells are color-coded according to *qualitative* comparison of each version's outcome to no correction. Red shades indicate improvement, blue deterioration. For white cells there was no considerable difference to the uncorrected case.

Overview nonlinear coregistration

Five sets of parameters are listed in Table 2, along with a broad outline of their outcomes. Improvements and deteriorations are presented in comparison to the uncorrected case. A more detailed discussion of the different aspects of evaluation in relation to fieldmap and topup correction is provided in the subsequent sections. V1 represents the set of core parameters that is closest to standard values for SyN transformation in ANTs. This setup yields promising results in terms of the derived group mask and the deformation fields for simulated data. Unfortunately, the remaining measures show worse outcomes for this version than for no correction; large shift and CR values indicate overfitting. To counteract this effect, deformations are limited more strictly to phase encoding direction in v2. While the restriction causes the outcomes to be less extreme, the general evaluation pattern remains. For a yet more conservative transformation, iterations are drastically reduced in v3. Evaluation of this version arguably yields the best overall picture, although the deformation fields exhibit reduced continuity. Additional strict limitation of deformation direction gives virtually the same results (cf. v6 in Supplementary Material). In v4 the deformation is further confined to

regions that generally show high fieldmap values (Gholipour et al. 2008b). This might carry the constraints too far, as the advantages over the uncorrected case further diminish. The same picture occurs for additional strict limitation of the deformation direction (v7 in Supplementary Material), while with increased iterations the restriction to the mask fails altogether (v8 and v9 in Supplementary Material) . In v5 B-spline regularization is employed to derive smoother deformation fields even with few iterations. Although the fields indeed present more continuous, their spatial pattern is absolutely unreasonable for real data, entailing consistently worse results in the evaluation. B-spline regularization does not yield satisfactory results in combination with any other parameter sets either (v10 - v16 in Supplementary Material).

Deformation fields

Deformation fields are evaluated using the subject's fieldmap and topup derived shiftmap or the ground truth distortion field as a reference. Overall, much closer resemblance to the reference field is achieved for the simulated than for the real data (Fig. 2a vs b). Because fields and correlations are highly similar between fieldmap and topup correction, Figure 2 only shows the results for the fieldmap based method for clarity. Outcomes for topup derived fields can be found in Supplementary Figure 5 and 7. Nonlinear coregistration with v1 parameter settings achieves a decent convergence with the reference field in the simulation, as showcased for an echo spacing of 0.7 ms in Figure 2a. Considering the full range of distortion levels, correlation values start low but monotonically increase up to almost 0.65 for an echo spacing of 1 ms (Fig. 2c). In stark contrast, the real data deformation fields differ drastically from the reference fields, as exemplified on a single subject in Figure 2b. The shifts partly even point in the opposite direction of the fieldmap which is reflected by negative correlation values (Fig. 2d). The span between maximum positive and negative shifts is higher than in the reference field for real data and simulated data with moderate distortions (Fig. 2d,e). Deformation fields generated with higher directional restriction in v2 appear very similar to v1 visually, but correlation values indicate worse correspondence to the reference field for the simulated data. The range of shift values is even larger than for v1 in both datasets. In v3 the reduction of iterations leads to reduced field continuity and shift values. However, the reference field correlation and spatial pattern are clearly improved for

real data and similar to v2 for simulated data. Fieldmap masking in v4 generates very low shift magnitudes even within the mask and low correlation to the reference fields. B-spline regularization in v5 positively impacts on the smoothness of the fields and increases shift magnitude. This however comes at the cost of declined spatial resemblance to the reference field.

Group masks

The minimal group EPI masks delineate which areas of the brain are covered by signal in the EPI image of each subject in the sample. The group mask after fieldmap correction illustrates an increased coverage across subjects of prefrontal and anterior temporal areas as well as posterior portions of the occipital lobe and the cerebellum (Fig. 3). However, more posterior regions of orbitofrontal and temporal cortex, as well as parts of hippocampus, amygdala and the pons are covered to a lesser extent by the group mask after fieldmap compared to no correction. In frontal areas, the mask seems to partially extend beyond the cortex. The group mask after topup correction shows a similar pattern, although differences to no correction are slightly less extreme. After nonlinear coregistration according to v1, the mask shows similar gains in frontal, temporal and cerebellar regions, but there is also an increased coverage in OFC and no decrease in subcortical regions. Strict limitation to phase encoding direction in v2 entails a mask shape similar to v1, although no increases occur in temporal and less in orbitofrontal regions. The same is true for restricted iterations in v3 and additional fieldmap masking in v4, although gains are generally even smaller. Finally, v5 with B-spline regularization yields almost no increase of group mask extents. The spatial variability of EPI masks across subjects as judged from mask group average and standard deviation reflect the patterns described for the minimal group mask above (not shown).

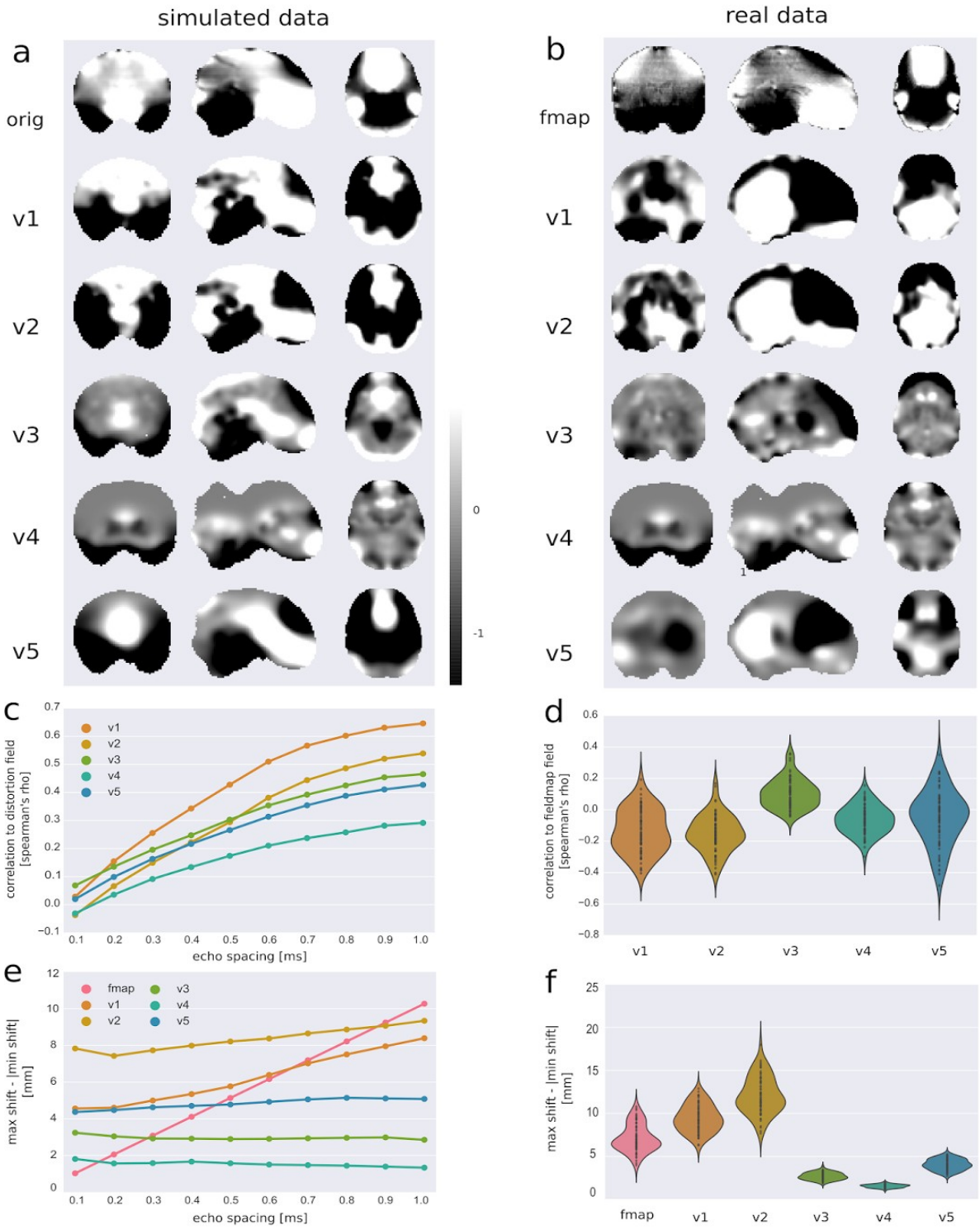

Figure 2. Deformation Fields. Shown are the outcomes of each correction method regarding the produced deformation fields for simulated *(first column)* and real data *(second column)*. Representative, masked maps of the shifts in phase encoding direction (x=-5, y=-14, z=18 mm) are shown for one level of distortion (0.7 ms echo spacing) (**a**) or for a single subject (**b**), respectively. For all 10 levels of distortion or across all 73 subjects respectively, **c** and **d** illustrate the voxelwise Spearman's rank correlation to the reference field (orig/fmap, all correlations two-sided $p < 0.001$). **e** and **f** depict the difference between the robust minimum and maximum shift values of the fields. orig=original distortion, fmap=fieldmap correction, v1-5=nonlinear correction (see Tab. 2)

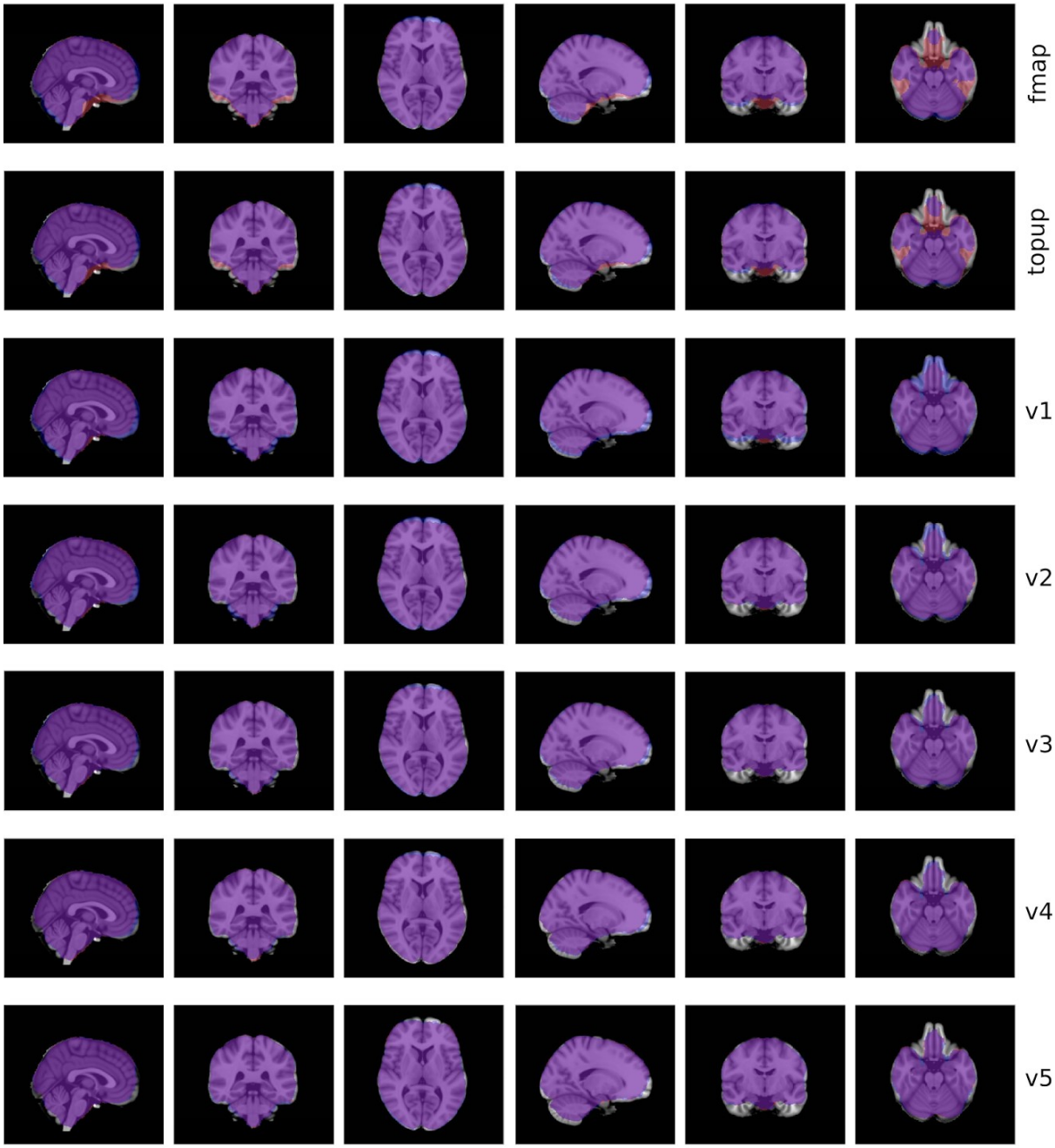

Figure 3. Minimal group masks. The products of all subjects' EPI masks after different correction methods are overlaid on the MNI152 1mm standard brain (N=73, from left to right x=2, y=-37, z=7, x=19, y=-8, z=22 mm). *Red* areas are exculsively covered by the groupmask without any correction, *blue* regions are only included after the images have undergone the correction indicated on the right, *purple* illustrates overlap of both masks. fmap=fieldmap correction, topup=topup correction, v1-5=nonlinear correction (see Tab. 2)

Similarity to anatomy

Visual inspection of the group average EPI image in relation to anatomical reference reveals two main aspects of fit, namely alignment of grey and white matter (gm/wm) boundaries and

fit to the outer brain contour. Figure 4a illustrates that both fieldmap and topup correction greatly improve gm/wm fit, exemplified on the genu of the corpus callosum which suffers substantial misregistration in the uncorrected image. While both corrections lead to a better fulfillment of the brain outline in prefrontal and partly in temporal regions, the discrepancy between EPI and T1w image in orbitofrontal areas increases. In line with these observations, group level EPI to T1w similarity as assessed by normalized mutual information (NMI) increases for the whole brain (Fig 4b, *first row*) but decreases when calculated within an OFC mask (Fig 4c, *first row*). Excessive deformation through v1 nonlinear coregistration matches the outer brain borders at the cost of massively corrupting gm/wm boundary fit. Moreover, a blurry group average indicates inconsistent results across subjects. These observations are in line with clearly reduced and widespread NMI values. Very high CR values imply overfitting based on the closely related cross correlation metric that was used for nonlinear registration. The group average of v2 is much clearer and shows better alignment of gm/wm boundaries, as the EPI images is not stretched in ventral direction. At the same time, this leads to worse outline fit in temporal regions. Whole brain NMI shows even lower values for v2 than for v1, while the CR values are less extreme. V3 with fewer iterations improves both gm/wm and outline fit compared to no correction, the former to a lesser and the latter to a greater extent than fieldmap and topup correction. This is also reflected in the NMI values. CR values are similar to v2. Restrictive masking in v4 results in slightly less improvement than achieved with v3. B-spline regularization in v5 yields worse outline fits and whole brain NMI values.

Direct comparison of corrected images

Global voxelwise correlation of each subject's EPI mean image across correction methods (including no correction) yields overall high values (Fig 5a). However, based on intensity difference maps, local distinctive features can be identified (Fig 5c) that support spatial patterns observed for the group masks and anatomical fit. Because outcomes from fieldmap and topup correction were again highly similar, only the results for fieldmap correction are shown here (for topup results see Supplementary Fig. 11 and 13). Subtraction of the uncorrected from the fieldmap corrected image illustrates increased signal intensity in temporal and prefrontal areas and small posterior portions of the cerebellar and occipital cortex after correction (Fig. 5c). In posterior OFC and around the genu of the corpus

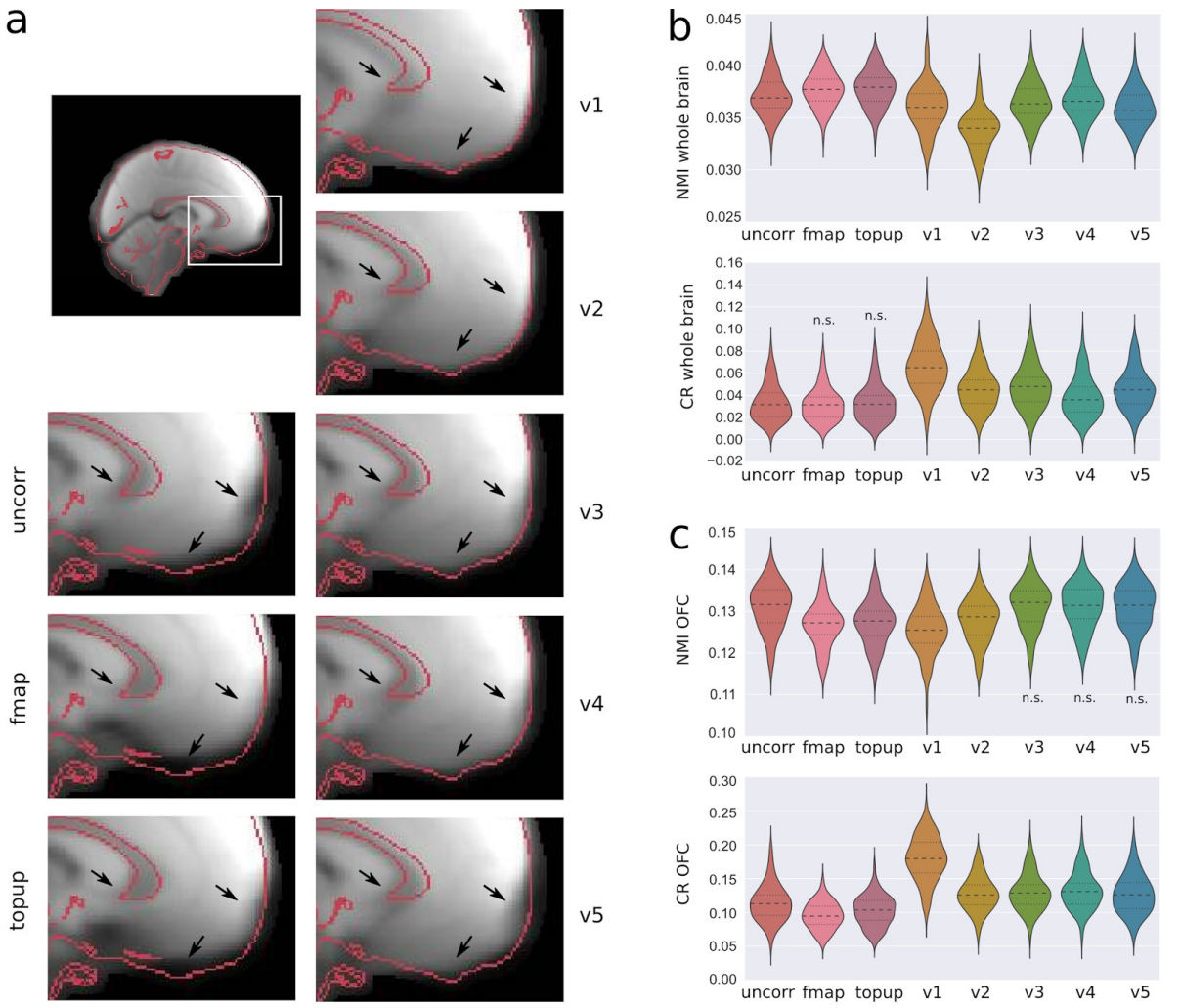

Figure 4. Similarity to anatomy. A group average of EPI mean images (N=73) is overlaid with the grey-white matter edges and brain mask outline of the MNI152 1 mm standard brain in **a**. Group distributions show the similarity between each subject's T1w and EPI image in terms of normalized mutual information (NMI) and correlation ratio (CR) within a whole brain (**b**) and OFC mask (**c**). For all but the indicated (n.s.) distributions the difference to the uncorrected case was significant ($p<0.001$, N=73). uncorr=uncorrected, fmap=fieldmap correction, topup=topup correction, v1-5=nonlinear correction (see Tab. 2)

callosum the intensity is decreased. Images corrected following v1 nonlinear coregistration show by far the lowest correlation to fieldmap corrected images (Fig. 5a). From the difference maps it becomes apparent that this correction involves drastic and widespread intensity changes. In particular the corpus callosum and the straight sinus obviously underwent major displacement. At the same time, the intensity decrease in OFC observed for fieldmap correction is absent. These findings are also reflected in the direct contrast of the fieldmap and nonlinearly corrected image (Fig 5c, *second column*). Deformation restriction in v2 alleviates the extreme intensity changes, suiting increased correlation values. The

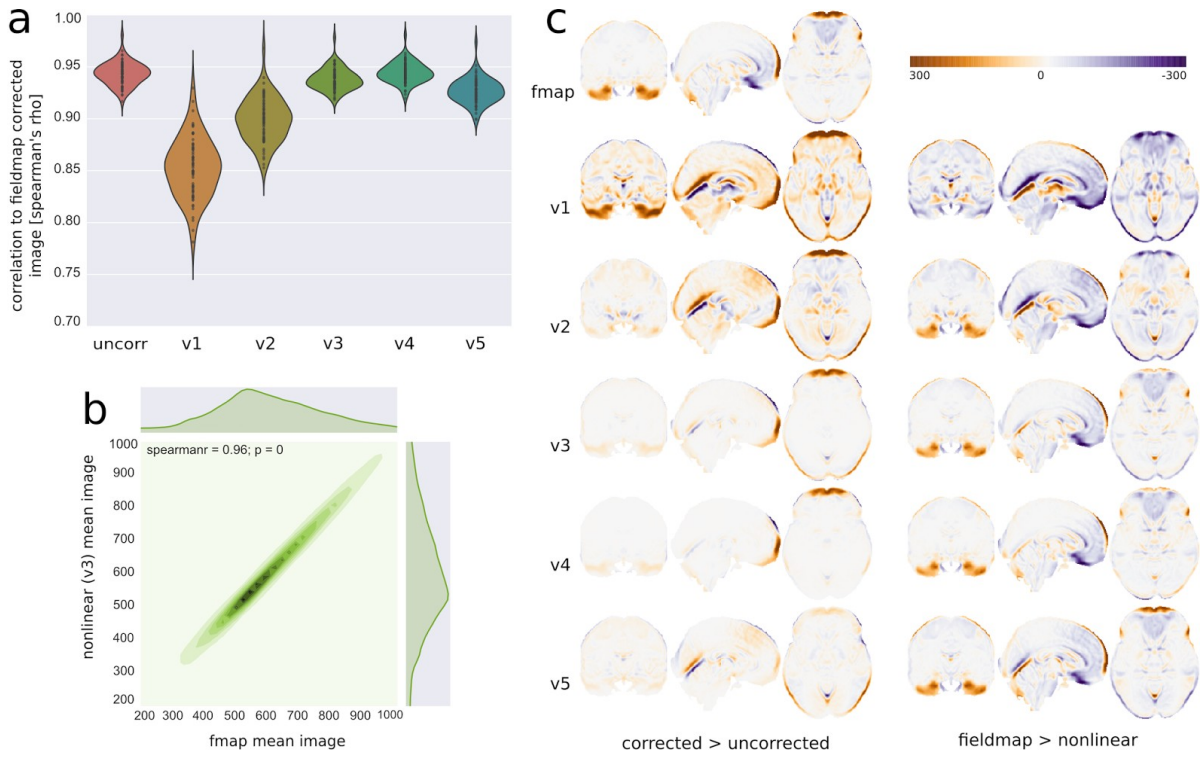

Figure 5. Comparison to other correction methods. The group distributions of voxelwise Spearman's rank correlation of the subjects' uncorrected (uncorr) or nonlinearly corrected (v1-5) to the fieldmap corrected (fmap) mean EPI image are shown in **a**. In **b** the mean EPI image of one subject after fieldmap correction is plotted against the image after nonlinear coregistration v3. The group level intensity difference maps are shown in **c**. They depict the result of subtracting the uncorrected from the corrected image (first column) or the nonlinearly corrected from the fieldmap corrected images (second column), respectively.

divergence in central areas remains, although it is more focused on straight sinus and the splenium of the corpus callosum. A major difference to v1 and fieldmap correction is the lack of intensity increase in temporal regions. While the latter issue also holds for v3, the reduction in iterations succeeds to limit differences mostly to pre- and orbitofrontal areas (yet without signal decrease in OFC). Only little deviations remain around the straight sinus, which are diminished by fieldmap masking in v4. Finally, with B-spline regularization in v5, nonlinear correction fails to produce intensity changes in areas affected by distortion and instead leads to signal displacement around the straight sinus. Intensity values of one subject's fieldmap and nonlinear (v3) corrected images are plotted against each other in Figure 5b.

Relation to ground truth

The simulated undistorted image is used as a ground truth for the arte

ificially distorted and subsequently corrected images. It is worth noting, that in this context, fieldmap correction represents unwarping with the exact same field that was used to distort the image in the first place. This procedure does not lead to a stainless recovery of the undistorted image, because standard fieldmap correction does not account for the intensity accumulations associated with geometric distortions (see Fig. 6b exemplifying visual inspection for one level of distortion). Likewise, fieldmap correction does restore ground truth correlation, especially for strong distortions, but not to the full extent (Fig. 6a). Nonlinear coregistration in most cases entails a decline in correlation values, especially for small to moderate distortions. Correction according to v1 leads to decreased correlation values for all levels of distortion. Although the visual impression of the correction is reasonable on the first glance, a closer look reveals that the image is excessively deformed in the ventral direction. Moreover, the signal in orbitofrontal regions appears to be stretched in posterior rather than anterior direction as would be appropriate judging from the distortion

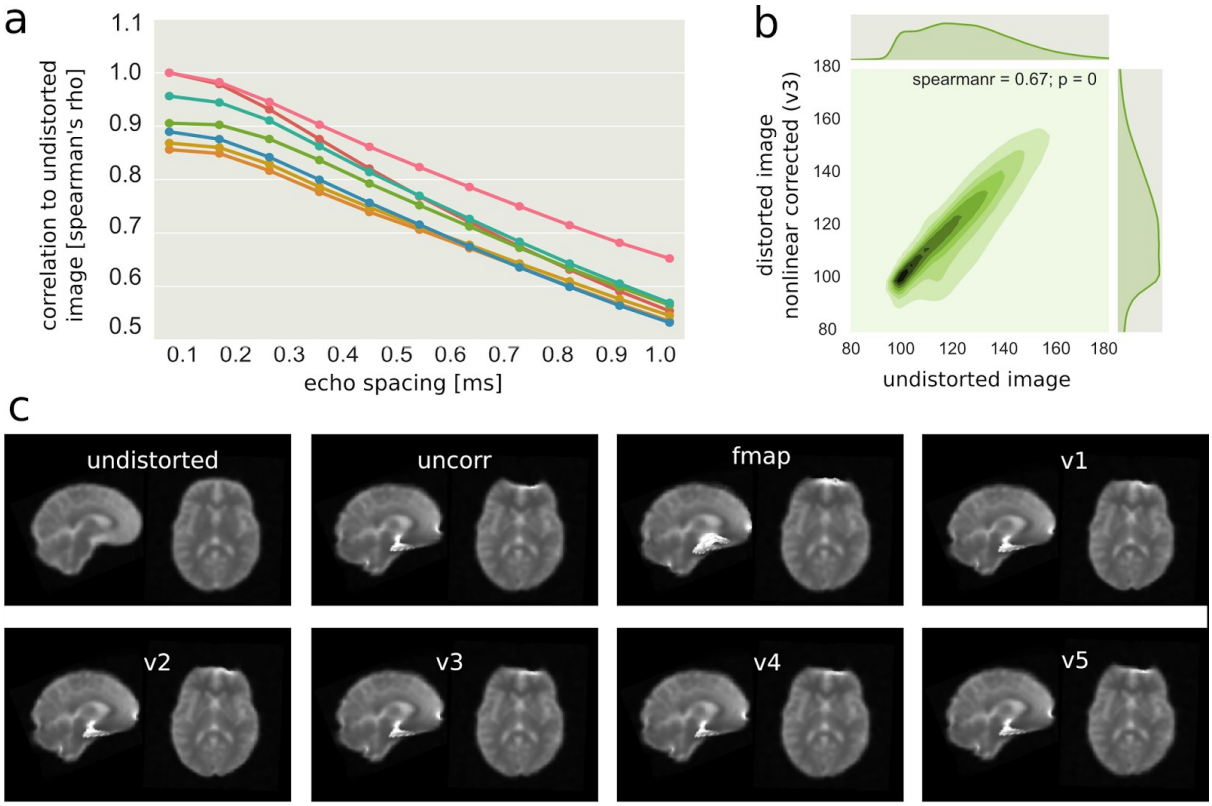

Figure 6. Ground truth comparison. The relation of differently corrected images to the undistorted image are shown in terms of voxelwise Spearman's rank correlation (**a,** all correlations two-sided $p < 0.001$), and visual inspection (**c,** echo spacing = 0.7 ms). For one level of distortion (0.7 ms), the v3 nonlinear corrected image is plotted against the undistorted image in **b**. uncorr=uncorrected, fmap=fieldmap, v1-5 = nonlinear correction (see Tab. 2)

field (see also Fig 2a, *first* vs *second row*). Correlation values for v2 closely resemble those for v1, while visually the deformations seem to be less extreme, especially in OFC. Restricted iterations in v3 still improve the visual appearance of the distorted image but to a lesser extent than fieldmap correction. Quantitatively, correlation values are slightly increased through the v3 correction for larger distortions (> 0.6 ms). Fieldmap masking in v4 gives a similar picture. B-spline regularization (v5) seems to entail favourable results in terms of the shape of the corpus callosum but not for frontal regions. Correlation to the ground truth is relatively low.

Discussion

The two main objectives underlying the present study were straightforward implementation and comprehensive large-scale evaluation of nonlinear coregistration for the correction of distortion artefacts. While these overall aims were met, the obtained results call into question the applicability of the investigated approach. The correction of distortion artefacts through nonlinear coregistration was not successful in general. However, considerable variation in the outcomes was observed across datasets and the employed measures partly diverged. The initial evaluation of similar methods usually relies on few images or artifical data and fails to capture the perfomance across larger and diverse datasets. The results obtained here highlight the importance of secondary exhaustive assessments of new approaches in terms of robustness and required conditions before the adoption to common analysis procedures can be considered.

User-friendly implementation with commonplace tools

While former studies on nonlinear coregistration focused on the development of suitable algorithms, the goal here was the translation into a practical preprocessing step. This was realized by integrating the popular normalization tool ANTs (Avants et al. 2011) and commands from other common neuroimaging software into a single easy-to-use pipeline with Nipype (Gorgolewski et al. 2011) (Fig. 1). The applied transformation model SyN (Avants et al. 2008) has been shown to outperform a number of available algorithms (Klein et al. 2009; Murphy et al. 2011) and explicitly enables large deformations like those required in the current use case. Importantly, this framework allows flexible parameter variation including

restriction of the deformation direction and B-Spline regularization (Tustison & Avants 2013). The pipeline only requires the EPI and surface extracted T1w image as inputs, whereas existing approaches often rely on additional scans derived with spin echo EPI (Studholme et al. 2000), high resolution gradient echo EPI (Gholipour et al. 2008a) or non-EPI (Villain et al. 2010) sequences. Computing the nonlinear transformation of a mean EPI image using the proposed pipeline only takes a few minutes, whereas others report computation times of about one hour (e.g. Gholipour et al. 2008a) .

Comprehensive evaluation employing multiple measures

The evaluation of accurate coregistration is not a trivial problem (Crum et al. 2004), especially in the case of EPI and T1w image pairs where typical procedures such as manual segmentation (Klein et al. 2009) are not feasible. Common practice is a combination of visual inspection and quantitative similarity metrics like mutual information (Hutton et al. 2002; Cusack et al. 2003). However, the former remains subjective and difficult for large samples[9] and the latter does not provide any anatomical meaning (Crum et al. 2004). In previous studies of nonlinear BOLD EPI and T1w coregistration, evaluation was usually limited to these two measures (Kybic et al. 2000; Gholipour et al. 2008a), although Studholme and colleagues additionally assessed the distance between manually placed landmarks (Studholme et al. 2000). The present study employed a greater variety of outcome measures to capture different aspects of registration quality. For instance, voxelwise correlation (Chambers et al. 2014) (Fig. 5a,b and 6a,b) and direct intensity differences (Fig. 5c) provided additional information about the corrected images. Careful examination of the deformation fields (Fig. 2) turned out to be a valuable tool to assess the quality and remaining issues of the transformation. The evaluation of minimal group masks (Fig. 3) addresses the pragmatic issue of compromised group level overlap due to different artefacts across individuals (Cusack et al. 2003). However, in the present context mask extents were not a reliable proxy for overall performance (cf. Tab. 2, results for v1 and v2). The comprehensive assessment came at the cost of a higher complexity of results, challenging overarching conclusions. Coincidentally, converging evidence across measures regarding spatial aspects of group masks, anatomical fit and intensity difference maps could strengthen ensuing conclusions and

[9] still "*careful visual inspection remains the first and most important validation check available for previously unseen data*" (Crum et al. 2004)

support validity of the single measures. Even divergence should not be considered a drawback as the additional information can foster a deeper understanding of the method and the results. For example, the two metrics used to measure EPI and T1w similarity yielded disturbingly divergent results, with CR diagnosing much higher similarity after nonlinear correction than NMI (Fig. 3b,c). This incoherence however, can be attributed to CR being closely related to the metric used for optimization during the transformation. It is worth noting, that all previous studies discussed above employ the same metric for optimization and correction, potentially limiting the informational content of respective measures.

Comparative approach in a large sample

Apart from a more extensive set of outcome measures the present study stands out from prior ones in terms of the employed dataset. In general, to improve feature control and establish a ground truth comparison, earlier studies relied on simulated (Kybic et al. 2000; Gholipour et al. 2008a) or phantom data (Studholme et al. 2000). Because such images do not reflect all characteristics of real data and the obtained results remain an approximation, evaluation is usually complemented with real data. Yet real datasets are typically confined to a few image pairs (Studholme et al. 2000; Gholipour et al. 2008a). While Kybic and colleagues claim their method was tested on "*several hundreds of images*", documented results shrink to the visual presentation of a single image with rather moderate distortions (Kybic et al. 2000). In contrast, the results presented here are based on a total of 73 real images acquired according to latest standards. Initial testing was performed on another set of over 300 images (Enhanced Nathan Kline Institute - Rockland Sample) (Nooner et al. 2012) which did not undergo full evaluation. Based on the large sample size, outcome measures could be obtained on the group level to assess the method's robustness and potential for widespread application. In fact, visual inspection of single subjects' corrected images partly appeared more reasonable than the obtained group level results would suggest. This indicates a lack of robustness across subjects and it is possible, that similar problems would be encountered if previous approaches were tested on larger samples. The dataset also comprised additional scans for fieldmap and reverse phase encoding based distortion correction. The proposed procedure could thus be evaluated in direct comparison to tried and tested approaches, which is of particular interest for guiding decisions in "real life" application. Again, this information is not contained in

most prior studies, although Kybic and colleagues compare their procedure to manual correction (Kybic et al. 2000). To exploit the aforementioned advantages of synthetic data, a simulation was performed in addition to the real data. Different from most prior approaches, a real fieldmap was used to introduce realistic distortions as proposed by Chambers and colleagues (Chambers et al. 2014). The evaluation outcomes differed considerably between simulated and real data (Tab. 2), most obviously illustrated for the deformation fields (Fig. 2a vs b). Potential reasons are manifold and include difference in resolution and smoothness as well as extreme intensity accumulations in the simulated data (see Supplementary Fig. 3). The latter implies that the nonlinear procedure could benefit from additional preprocessing to overcome intensity nonuniformity (Chambers et al. 2014). In any case, these observations underline the importance of thorough evaluation also based on real data.

Nonlinear coregistration: issues and insights

Nonlinear coregistration of BOLD EPI and T1w images within the proposed framework turned out much more challenging than expected. First, a suitable preprocessing procedure had to be set up to render the images suitable for direct coregistration (Fig. 1b). Because of the multitude of (interacting) parameters in ANTs, extensive testing was required to find reasonable settings. Throughout the testing process there emerged a general trade off between the need for large deformations in affected areas on the one hand and unreasonable results produced by unconstrained transformation on the other (cf. Tab. 2). Different approaches were pursued to address this issue. Following Gholipour and colleagues, deformations were restricted to phase encoding direction (Gholipour et al. 2008a). However, only when convergence was prohibited through the reduction of iterations, the outcomes were notably improved (v3). Because this approach conversely did not achieve sufficient correction, an alternative idea was to allow convergence, but only within a mask comprising regions that typically show high values in fieldmaps (Supplementary Fig. 1). Unfortunately, ANTs was very sensitive regarding image masking; the expected spatial restriction could not be realized for a high number of iterations (cf. v8 and v9 in Supplementary Material) and posed too high constraints when combined with few iterations (v4). While explicit B-Spline regularization of the deformation fields succeeded to enforce physically plausible smoothness, no satisfactory correction could be obtained (v5 and v10 - v16 in Supplementary Material). This is surprising

in so far, as previous approaches successfully use spline based estimation (Kybic et al. 2000; Studholme et al. 2000; Gholipour et al. 2008a). A possible explanation is that with 26 mm the initial knot spacing was set too high and supported registration of far apart image features in the absence of sufficient information in the EPI image (Studholme et al. 2000).

While nonlinear coregistration in general performed drastically worse than fieldmap and topup correction, one distinctive feature stands out, that on the first glance could be deemed an advantage. EPI signal coverage and similarity to the structural image decreased through fieldmap and topup correction in the OFC, while they mostly increased with nonlinear coregistration (Fig. 3 and 4). However, this observation can probably be explained by actual signal loss in the OFC due to spin dephasing within single voxels (Ojemann et al. 1997; Glover 1999). Distortions and dropout are related but distinct phenomena and the latter is usually not addressed by retrospective correction methods discussed here (although see Jenkinson 2004). It seems likely that fieldmap and topup corrected images accurately reflect the signal loss, while nonlinear coregistration attempts to overcome this loss by artificially stretching signal into the affected regions. This is in line with poor results for the case of simulated signal loss reported by Gholipour and colleagues (Gholipour et al. 2008a). Given the observed extension of EPI signal beyond the brain particularly after fieldmap correction (Fig 3 *second row*), it is possible but not highly likely that a tendency for overcorrection brings about more signal decrease in OFC than would be appropriate.

Limitations and future directions

The limitations of the proposed method are obvious and should discourage its premature use. Importantly, the presented results pertain to the specific procedure and tools that used here and do not necessarily hold for alternative implementations. Notwithstanding the current issues, the basic idea of nonlinear coregistration for distortion correction bears potential and should continue to be explored. An interesting approach has been suggested by Gholipour and colleagues (Gholipour 2008c). They use a fieldmap template for an initial coarse round of deformation which is subsequently refined through nonlinear coregistration. Thus the critical gross displacements are dealt with by the fieldmap while nonlinear transformation provides accurate individual alignment. However, this procedure depends on a reasonable fieldmap template. Future work might establish to what extent such a template generalizes

across studies and can circumvent the need for additional scans. Along similar lines, Daga and colleagues (Daga et al. 2013) proposed an elegant procedure combining phase unwrapping with confidence estimation regarding the obtained B0 field to confine the following nonlinear registration to low confidence areas. While the latter approach does not obliviate fieldmap acquisition, the combination of methods holds additional potential to overcome a considerable drawback of fieldmap (and topup) based procedures: due to their static nature fieldmaps cannot account for artefacts arising from the interaction of distortion and subject movement (Andersson et al. 2001; Jezzard 2012). Fieldmap correction followed by individual nonlinear refinement of each volume in a time series could be a solution. Another objective of future research should be to assess the impact of nonlinear coregistration, and distortion correction in general, on subsequent function analyses. This has been addressed to some extent in terms of task-based activations (Cusack et al. 2003; Villain et al. 2010) and an attempt to assess changes in resting state functional connectivity was made in the context of the current project (see Supplementary Fig. 15). However, both approaches suffer from the absence of a ground truth comparison. As distortion artefacts increase with field strength (Dietrich et al. 2008), adequate correction will gain importance with the current rise of ultra high field fMRI (Jezzard 2012). Remarkable improvements in contrast and resolution that can be achieved with EPI sequences at 7 Tesla might at the same time call for and facilitate nonlinear coregistration.

Conclusion

Direct nonlinear BOLD EPI to T1w coregistration was implemented in a user-friendly framework and thoroughly evaluated on a large dataset. Despite extensive attempts to optimize the correction, no satisfactory results could be obtained. The trade off between large deformations and suitable constraints as well as the lack of robustness across subjects and data types emerged as the prevailing issues. While the former problem might be overcome with more specifically tailored transformation algorithms or a combination with general information from fieldmaps, the latter concern is potentially harder to address. In the face of individual differences in distortions and varying image quality, robust automatization of nonlinear BOLD EPI and T1w coregistration is difficult to achieve. On these grounds extensive critical evaluation of respective approaches is of crucial importance.

Acknowledgments

I am grateful for excellent supervision by Daniel S. Margulies and Felix Blankenburg as well as for outstanding methodological guidance by Chris Gorgolewski, Alfred Anwander, Jan Schreiber, Pierre-Louis Bazin and Mark Jenkinson. Special thanks belong to the LEMON crew for providing the data, Ali Gholipour for sharing the fieldmap template and to the Group for Neuroanatomy and Connectivity at the MPI CBS Leipzig.

Supplementary material

The supplementary material can be found in an accompanying file and online under http://goo.gl/JIqFpH

References

Andersson, J.L. et al., 2001. Modeling geometric deformations in EPI time series. *NeuroImage*, 13(5), pp.903–919.

Andersson, J.L.R., Skare, S. & Ashburner, J., 2003. How to correct susceptibility distortions in spin-echo echo-planar images: application to diffusion tensor imaging. *NeuroImage*, 20(2), pp.870–888.

Avants, B.B. et al., 2011. A reproducible evaluation of ANTs similarity metric performance in brain image registration. *NeuroImage*, 54(3), pp.2033–2044.

Avants, B.B. et al., 2008. Symmetric diffeomorphic image registration with cross-correlation: evaluating automated labeling of elderly and neurodegenerative brain. *Medical image analysis*, 12(1), pp.26–41.

Bazin, P.-L. et al., 2014. A computational framework for ultra-high resolution cortical segmentation at 7Tesla. *NeuroImage*, 93 Pt 2, pp.201–209.

Bhushan, C. et al., 2012. Correcting Susceptibility-Induced Distortion in Diffusion-Weighted MRI using Constrained Nonrigid Registration. In *Signal Information Processing Association Annual Summit and Conference (APSIPA ASC)*. pp. 1–9.

Brett, M., Johnsrude, I.S. & Owen, A.M., 2002. The problem of functional localization in the human brain. *Nature reviews. Neuroscience*, 3(3), pp.243–249.

Carass, A. et al., 2011. Simple paradigm for extra-cerebral tissue removal: algorithm and analysis. *NeuroImage*, 56(4), pp.1982–1992.

Chambers, M.C. et al., 2014. Registration-Based Distortion and Intensity Correction in fMRI.

Chen, N.K. & Wyrwicz, A.M., 1999. Correction for EPI distortions using multi-echo gradient-echo imaging. *Magnetic resonance in medicine: official journal of the Society of Magnetic Resonance in Medicine / Society of Magnetic Resonance in Medicine*, 41(6), pp.1206–1213.

Crum, W.R., Hartkens, T. & Hill, D.L.G., 2004. Non-rigid image registration: theory and practice. *The British journal of radiology*, 77 Spec No 2, pp.S140–53.

Cusack, R., Brett, M. & Osswald, K., 2003. An evaluation of the use of magnetic field maps to undistort echo-planar images. *NeuroImage*, 18(1), pp.127–142.

Daga, P. et al., 2013. Susceptibility artefact correction by combining B0 field maps and non-rigid registration using graph cuts. In *SPIE Medical Imaging*. International Society for Optics and Photonics, p. 86690B–86690B–6.

Dale, A.M., Fischl, B. & Sereno, M.I., 1999. Cortical surface-based analysis. I. Segmentation and surface reconstruction. *NeuroImage*, 9(2), pp.179–194.

Dietrich, O., Reiser, M.F. & Schoenberg, S.O., 2008. Artifacts in 3-T MRI: physical background and reduction strategies. *European journal of radiology*, 65(1), pp.29–35.

Drobnjak, I., Pell, G.S. & Jenkinson, M., 2010. Simulating the effects of time-varying magnetic fields with a realistic simulated scanner. *Magnetic resonance imaging*, 28(7), pp.1014–1021.

Fischl, B., Sereno, M.I. & Dale, A.M., 1999. Cortical surface-based analysis. II: Inflation, flattening, and a surface-based coordinate system. *NeuroImage*, 9(2), pp.195–207.

Gholipour, A. et al., 2008b. Average field map image template for Echo-Planar image analysis. *Conference proceedings: ... Annual International Conference of the IEEE Engineering in Medicine and Biology Society. IEEE Engineering in Medicine and Biology Society. Conference*, 2008, pp.94–97.

Gholipour, A. et al., 2007. Brain functional localization: a survey of image registration techniques. *IEEE transactions on medical imaging*, 26(4), pp.427–451.

Gholipour, A. et al., 2008c. Cross-Validation of Deformable Registration With Field Maps in Functional Magnetic Resonance Brain Imaging. *IEEE journal of selected topics in signal processing*, 2(6), pp.854–869.

Gholipour, A. et al., 2008a. Validation of non-rigid registration between functional and anatomical magnetic resonance brain images. *IEEE transactions on biomedical engineering*, 55(2 Pt 1), pp.563–571.

Glover, G.H., 1999. 3D z-shim method for reduction of susceptibility effects in BOLD fMRI. *Magnetic resonance in medicine: official journal of the Society of Magnetic Resonance in Medicine / Society of Magnetic Resonance in Medicine*, 42(2), pp.290–299.

Gorgolewski, K. et al., 2011. Nipype: a flexible, lightweight and extensible neuroimaging data processing framework in python. *Frontiers in neuroinformatics*, 5, p.13.

Greve, D.N. & Fischl, B., 2009. Accurate and robust brain image alignment using boundary-based registration. *NeuroImage*, 48(1), pp.63–72.

Holland, D., Kuperman, J.M. & Dale, A.M., 2010. Efficient correction of inhomogeneous static magnetic field-induced distortion in Echo Planar Imaging. *NeuroImage*, 50(1), pp.175–183.

Hutton, C. et al., 2002. Image distortion correction in fMRI: A quantitative evaluation. *NeuroImage*, 16(1), pp.217–240.

Jenkinson, M. et al., 2012. FSL. *NeuroImage*, 62(2), pp.782–790.

Jenkinson, M. et al., 2002. Improved optimization for the robust and accurate linear registration and motion correction of brain images. *NeuroImage*, 17(2), pp.825–841.

Jenkinson, M., 2004. Improving the registration of B0-distorted EPI images using calculated cost function weights.

Jenkinson, M. & Smith, S., 2001. A global optimisation method for robust affine registration of brain images. *Medical image analysis*, 5(2), pp.143–156.

Jezzard, P., 2012. Correction of geometric distortion in fMRI data. *NeuroImage*, 62(2), pp.648–651.

Jezzard, P. & Balaban, R.S., 1995. Correction for geometric distortion in echo planar images from B0 field variations. *Magnetic resonance in medicine: official journal of the Society of Magnetic Resonance in Medicine / Society of Magnetic Resonance in Medicine*, 34(1), pp.65–73.

Jezzard, P. & Clare, S., 1999. Sources of distortion in functional MRI data. *Human brain mapping*, 8(2-3), pp.80–85.

Klein, A. et al., 2009. Evaluation of 14 nonlinear deformation algorithms applied to human brain MRI registration. *NeuroImage*, 46(3), pp.786–802.

Kybic, J. et al., 2000. Unwarping of unidirectionally distorted EPI images. *IEEE transactions on medical imaging*, 19(2), pp.80–93.

Lucas, B.C. et al., 2010. The Java Image Science Toolkit (JIST) for rapid prototyping and publishing of neuroimaging software. *Neuroinformatics*, 8(1), pp.5–17.

Mansfield, P., 1977. Multi-planar image formation using NMR spin echoes. *Journal of Physics C: Solid State Physics*, 10(3), p.L55.

McAuliffe, M.J. et al., 2001. Medical Image Processing, Analysis and Visualization in clinical research. In *Computer-Based Medical Systems, 2001. CBMS 2001. Proceedings. 14th IEEE Symposium on*. pp. 381–386.

Murphy, K. et al., 2011. Evaluation of registration methods on thoracic CT: the EMPIRE10 challenge. *IEEE transactions on medical imaging*, 30(11), pp.1901–1920.

Nooner, K.B. et al., 2012. The NKI-Rockland Sample: A Model for Accelerating the Pace of Discovery Science in Psychiatry. *Frontiers in neuroscience*, 6, p.152.

Ogawa, S. et al., 1990. Brain magnetic resonance imaging with contrast dependent on blood oxygenation. *Proceedings of the National Academy of Sciences of the United States of America*, 87(24), pp.9868–9872.

Ojemann, J.G. et al., 1997. Anatomic localization and quantitative analysis of gradient refocused echo-planar fMRI susceptibility artifacts. *NeuroImage*, 6(3), pp.156–167.

Reber, P.J., Wong, E.C. & Buxton, R.B., 1998. Correction of off resonance-related distortion in echo-planar imaging using EPI-based field maps. *Magnetic resonance insights*.

Smith, S.M. et al., 2004. Advances in functional and structural MR image analysis and implementation as FSL. *NeuroImage*, 23 Suppl 1, pp.S208–19.

Smith, S.M., 2002. Fast robust automated brain extraction. *Human brain mapping*, 17(3), pp.143–155.

Studholme, C., Constable, R.T. & Duncan, J.S., 2000. Accurate alignment of functional EPI data to anatomical MRI using a physics-based distortion model. *IEEE transactions on medical imaging*, 19(11), pp.1115–1127.

Tao, R. et al., 2009. A variational image-based approach to the correction of susceptibility artifacts in the alignment of diffusion weighted and structural MRI. *Information processing in medical imaging: proceedings of the ... conference*, 21, pp.664–675.

Toga, A.W. & Thompson, P.M., 2001. The role of image registration in brain mapping. *Image and vision computing*, 19(1-2), pp.3–24.

Tustison, N.J. & Avants, B.B., 2013. Explicit B-spline regularization in diffeomorphic image registration. *Frontiers in neuroinformatics*, 7, p.39.

Villain, N. et al., 2010. A simple way to improve anatomical mapping of functional brain imaging. *Journal of neuroimaging: official journal of the American Society of Neuroimaging*, 20(4), pp.324–333.

Weisskoff, R.M. & Davis, T.L., 1992. Correcting gross distortion on echo planar images. *11th Ann. Sci. Mtg. Soc. of Magn. Reson. in Med.*

Wu, M. et al., 2008. Comparison of EPI distortion correction methods in diffusion tensor MRI using a novel framework. *Medical image computing and computer-assisted intervention: MICCAI ... International Conference on Medical Image Computing and Computer-Assisted Intervention*, 11(Pt 2), pp.321–329.

Zhang, Y., Brady, M. & Smith, S., 2001. Segmentation of brain MR images through a hidden Markov random field model and the expectation-maximization algorithm. *IEEE transactions on medical imaging*, 20(1), pp.45–57.

Erklärung

Hiermit erkläre ich, dass ich vorliegende Arbeit selbständig verfasst und keine anderen als die angegebenen Quellen und Hilfsmittel benutzt habe.

…….....

Berlin, 20. August 2014